

# Nucleation, Growth, and Form in Crystals of Peptide Helices

Prema G. Vasudev,<sup>†</sup> Narayanaswamy Shamala,<sup>\*,†</sup> and Padmanabhan Balaram<sup>\*,‡</sup>

Department of Physics, Indian Institute of Science, Bangalore 560 012, India, and Molecular Biophysics Unit, Indian Institute of Science, Bangalore 560 012, India

Received: September 9, 2007; In Final Form: October 22, 2007

A model for the nucleation of crystallization in peptide helices is presented. The crystal structures of four polymorphic forms of a hydrophobic helical decapeptide Boc–Leu–Aib–Phe–Phe–Leu–Aib–Ala–Ala–Leu–Aib–OMe (**I**) exemplify alternative packing modes in cylindrical molecules. Three crystal forms of peptide **I** are monoclinic  $P2_1$ , while one is orthorhombic  $P2_21_21$ . The five different helical molecules characterized have very similar backbone conformations over much of the peptide length. A survey of 117 helical peptide structures with a length  $\geq 8$  residues reveals a preponderance of the triclinic ( $P1$ ), monoclinic ( $P2_1$ ), and orthorhombic ( $P2_21_21$ ) crystal forms. Models for the formation of critical nuclei are based on helix association driven by solvophobic forces, resulting in the formation of raftlike structures. Raft association can be further driven by the imperative of minimizing solvent accessible surface area with the formation of blocks, which can be subsequently fitted in Lego set fashion by multiple hydrogen bond interactions in the head-to-tail region. This model provides a rationalization for observed crystal formation based on a postulated structure for an embryonic nucleus, which is determined by aggregation patterns and unconstrained by the dictates of symmetry.

## Introduction

Crystallization, the development of an ordered solid phase from a solution, depends on the formation of microscopic aggregates that serve as critical nuclei. The processes of nucleation and growth of crystalline phases have been extensively investigated theoretically.<sup>1,2</sup> However, obtaining experimental evidence for the structure of a crystal in its embryonic form is a formidable task, although recent attempts at visualizing nuclei using atomic force microscopy suggest that “advanced nucleation theories must treat the critical nucleus as a variable”.<sup>3</sup> The occurrence of polymorphic forms is undoubtedly indicative of variable modes of association in nascent nuclei.<sup>4</sup> A rapidly growing body of crystal structures of apolar helical peptides<sup>5,6</sup> presents an opportunity to revisit the “crystallization nucleus structure” problem by examining packing modes. The propensity of  $\alpha$ -aminoisobutryl (Aib) residue to promote helical folding in peptides has been exploited for three decades in the design of crystalline peptide helices.<sup>7–10</sup> An analysis of the packing modes of helices in crystals revealed important elements of molecular assembly resulting in the observed crystal forms.<sup>11</sup>

We present a nucleation model based on polymorphic helical structures, viewed as a problem of packing cylinders to satisfy the constraints of space group symmetry. The structures chosen may be approximated as uncharged cylinders, with irregular knoblike projections representing the side chains. Hydrogen bonding between free C=O and N–H groups at the helix termini and van der Waals interactions between side chains are the predominant forces which determine molecular arrangements within aggregates. The formation of raftlike structures permits

growth in two-dimensions with the piling of rafts resulting in propagation along the third dimension. Anisotropy of crystal growth and specific symmetries of molecular arrangements emerge readily from simple packing considerations, following D’Arcy Thompson’s dictum, first enunciated in 1917, that “it has come to be understood that the symmetrical conformation of a homogeneous crystalline structure is sufficiently explained by the mere mechanical fitting together of appropriate structural units along the easiest and simplest lines of ‘close packing’”.<sup>12</sup>

## Experimental Methods

Peptide **I** was synthesized by conventional solution-phase procedures using a fragment condensation strategy. Boc and methyl ester groups were used as N- and C-terminal protecting groups, respectively. Peptide couplings were mediated by  $N,N'$ -dicyclohexylcarbodiimide (DCC) and 1-hydroxybenzotriazole. The peptide was purified by reverse-phase medium-pressure liquid chromatography (C<sub>18</sub>, 40–60  $\mu$ m) using methanol/water gradients and characterized by 500-MHz <sup>1</sup>H NMR spectroscopy and matrix-assisted laser desorption–ionization mass spectrometry.

Two polymorphic crystal forms of the peptide were obtained by slow evaporation of 85% methanol/water (**Ia**) and 95% methanol/water (**Ib**). Preliminary crystallographic characterization of the crystals indicated the successful crystallization of polymorphic forms and that both the forms were monoclinic with slightly different cell parameters. Both the crystals belonged to space group  $P2_1$ . The third polymorph, **Ic**, was obtained by redissolving crystals of **Ia** in an isopropanol/water mixture. Slow evaporation yielded crystals (**Ic**) in orthorhombic space group  $P2_21_21$ . Polymorph **Id** was obtained by redissolving crystals of **Ib** in isopropanol to yield tiny crystals, which were dissolved in methanol/dioxane. Small crystals obtained were redissolved in isopropanol/water to yield crystals (**Id**) in the monoclinic space group  $P2_1$ . X-ray intensity data for the peptide crystals

\* To whom correspondence should be addressed. Phone: 91-80-22932856. Fax: 91-80-23602602/91-80-23600683. E-mail: shamala@physics.iisc.ernet.in (N.S.). Phone: 91-80-22932337. Fax: 91-80-23600683/91-80-23600535. E-mail: pb@mbu.iisc.ernet.in (P.B.).

<sup>†</sup> Department of Physics, Indian Institute of Science.

<sup>‡</sup> Molecular Biophysics Unit, Indian Institute of Science.

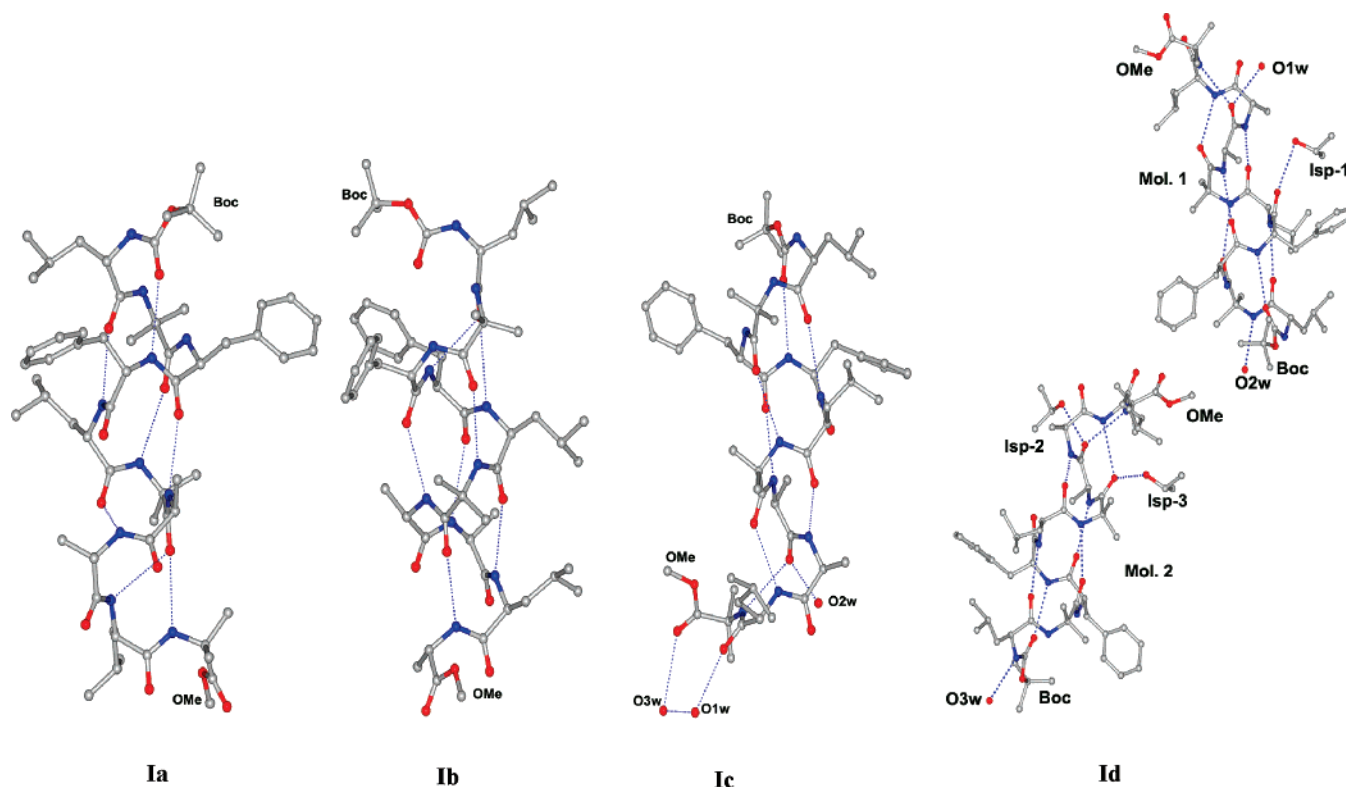


**Figure 1.** Molecular conformation of the decapeptide Boc-Leu-Aib-Phe-Phe-Leu-Aib-Ala-Ala-Leu-Aib-OMe (**I**) in four polymorphic crystals **Ia**, **Ib**, **Ic**, and **Id**. Hydrogen bonds are shown as dotted lines.

**TABLE 1: Crystal and Diffraction Parameters for the Polymorphs of Peptide I**

	<b>Ia</b>	<b>Ib</b>	<b>Ic</b>	<b>Id</b>
empirical formula	C <sub>60</sub> H <sub>94</sub> N <sub>10</sub> O <sub>13</sub>	C <sub>60</sub> H <sub>94</sub> N <sub>10</sub> O <sub>13</sub>	C <sub>60</sub> H <sub>94</sub> N <sub>10</sub> O <sub>13</sub> ·3H <sub>2</sub> O	C <sub>60</sub> H <sub>94</sub> N <sub>10</sub> O <sub>13</sub> ·3H <sub>2</sub> O·3C <sub>3</sub> H <sub>7</sub> OH
crystal habit	plates	rectangular	rectangular	rectangular
crystal size (mm)	0.22 × 0.15 × 0.02	0.33 × 0.26 × 0.13	0.34 × 0.11 × 0.05	0.5 × 0.3 × 0.08
crystallizing solvent	85% methanol/water	95% methanol/water	isopropanol/water	isopropanol/water
space group	<i>P</i> 2 <sub>1</sub>	<i>P</i> 2 <sub>1</sub>	<i>P</i> 2 <sub>2</sub> 2 <sub>1</sub>	<i>P</i> 2 <sub>1</sub>
<i>a</i> (Å)	11.292(6)	14.089(2)	10.760 (4)	10.886(2)
<i>b</i> (Å)	18.755(11)	15.386(3)	19.109(6)	18.755(4)
<i>c</i> (Å)	16.892(9)	17.097(3)	34.104(12)	36.427(8)
$\beta$ (deg)	103.77(1)	113.32(1)	90	96.93(1)
<i>Z</i>	2	2	4	4
volume (Å <sup>3</sup> )	3474(3)	3399.5(10)	7012(4)	7383(3)
molecules/asymmetric unit	1	1	1	2
cocrystallized solvent	none	none	3 water	3 water + 3 isopropanol
molecular weight	1163.45	1163.45	1211.45	1269.03
$\rho$ (g/cm <sup>3</sup> )(calcd)	1.112	1.137	1.147	1.142
<i>F</i> (000)	1256	1256	2608	2730
radiation	Mo K $\alpha$	Mo K $\alpha$	Mo K $\alpha$	Mo K $\alpha$
2 $\theta$ max (deg)	52.6	52.8	45.0	53.26
measured reflections	24857	24656	9127	24812
unique reflections	6639	6604	5099	14454
observed reflections [  <i>F</i>   g 4s(  <i>F</i>  )]	3804	5264	1615	10681
final R/wR2 (%)	8.87/13.55	6.03/12.9	10.7/21.6	13.3/34.7
GOF (S)	1.161	1.216	1.144	1.428
$\Delta\rho_{\max}/\Delta\rho_{\min}$ (e <sup>−</sup> ·Å <sup>−3</sup> )	0.34/−0.14	0.19/−0.15	0.22/−0.21	0.64/−0.43
restraints/parameters	1/748	1/748	15/776	22/1632
data-to-parameter ratio	8.8: 1	8.8: 1	6.5: 1	8.8: 1

were collected on a Bruker AXS SMART APEX CCD Diffractometer at room temperature using Mo K $\alpha$  radiation ( $\lambda = 0.71073$  Å).  $\omega$ -Scan type was used for collecting the data. The structures of the four polymorphs of the peptide were obtained by direct methods using SHELXD.<sup>13</sup> Least-squares refinement for all the structures were carried out against *F*<sup>2</sup> using SHELXL-97.<sup>14</sup> For **Ic** and **Id**, refinement was carried out in block-diagonal fashion. All the hydrogen atoms were fixed in idealized positions and refined in the final cycle as riding over the atoms to which they were bonded. The final *R* factor was 0.0887 (*wR2* =

0.1355) for 3804 observed reflections, with  $|F_o| \geq 4\sigma(|F_o|)$  for **Ia**. For **Ib**, the final *R* factor was 0.0603 (*wR2* = 0.129) for 5264 observed reflections, with  $|F_o| \geq 4\sigma(|F_o|)$ . For the polymorph **Ic**, restraints were applied on bond lengths and bond angles of the Leu (9) side chain in the refinement procedure. The final *R* value obtained was 0.1074 (*wR2* = 0.2159) for 1615 observed reflections, with  $|F_o| \geq 4\sigma(|F_o|)$ . Since twinning was detected in the data of **Id**, refinement was carried out in SHELXL using HKLF5 command. Application of the twin operator (−1 0 0/0 −1 0/0.808 0 1) obtained from the program

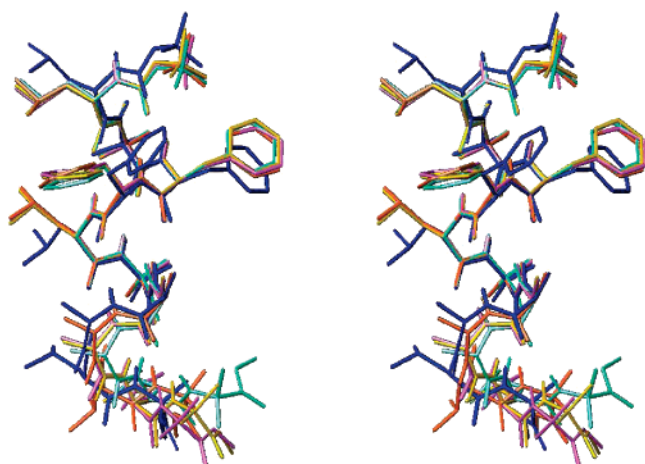


**Figure 2.** Stereoview of the superposition of five independent molecular conformations of peptide **I** determined in the four polymorphic crystals. Backbone atoms from N1 to N7 of **Ia** (orange), **Ib** (blue), **Ic** (pale green), **Id**, Mol. 1 (pink), and **Id**, Mol. 2 (yellow) are used for superposition (rmsd = 0.1 Å).

TWINROT<sup>15</sup> reduced the final *R* factor to 13.3% (*wR*<sub>2</sub> = 0.3468) for 10681 reflections with  $|F_o| \geq 4\sigma(|F_o|)$ . The domain fractions refined to 0.7 and 0.3 for the two domains. DFIX restraints were applied to the three isopropanol molecules in the final refinement cycle. The crystal and diffraction parameters are summarized in Table 1. The atomic coordinates have been deposited in the Cambridge Structural Database, with deposition numbers 648860–648863. These data can be obtained free of charge via [www.ccdc.cam.ac.uk/conts/retrieving.html](http://www.ccdc.cam.ac.uk/conts/retrieving.html) (or from the Cambridge Crystallographic Data Centre, 12 Union Road, Cambridge CB21EZ, UK; fax: (+44) 1223–336–033; e-mail: [deposit@ccdc.cam.ac.uk](mailto:deposit@ccdc.cam.ac.uk)). A dataset of 117 hydrophobic helical peptide crystal structures of length  $\geq 8$  residues was extracted from the Cambridge Structural Database (CSD).

## Results and Discussion

Figure 1 illustrates the molecular conformations of the decapeptide Boc–Leu–Aib–Phe–Phe–Leu–Aib–Ala–Ala–Leu–Aib–OMe (**I**) in four distinct polymorphic crystals. In all four cases the peptide backbone conformation is very similar as seen from the superposition of structures shown in Figure 2. An rmsd of 0.1 Å is obtained for the superposition of backbone atoms from N1 to N7. The backbone and side chain torsion

angles are listed in Table 2. The major differences in the backbone are observed near the C-terminus at the Leu (9) residue with significant change seen in the  $\phi$ ,  $\psi$  angles in polymorph **Ic**. At the level of side chains differences are observed for the Leu (1), Phe (4), and Leu (5) residues in **Ib** and Leu (9) in **Ia**. The backbone hydrogen-bonding patterns observed reveal a mixture of 4  $\rightarrow$  1 ( $3_{10}$  helical) and 5  $\rightarrow$  1 ( $\alpha$  helical) C=O...HN interactions. Transitions between the  $3_{10}$  and  $\alpha$  helical hydrogen-bonding patterns can be achieved without large positional changes of the backbone atoms. In our subsequent discussion of packing modes, we have approximated all four molecules as cylinders. The crystal structures of four polymorphic forms (three in monoclinic  $P2_1$  and one in orthorhombic  $P2_22_1$ ) of the decapeptide **I** illustrate the multiple modes of association of the cylindrical molecules in single crystals (Figures 3 and 4). A survey of the Cambridge Structural Database provides 117 examples of hydrophobic helices with a length  $\geq 8$  residues. Figure 5 summarizes the distributions of the observed crystallographic space groups. The monoclinic space group  $P2_1$  is most frequently observed (43 examples), followed by orthorhombic  $P2_12_12_1$  (33 examples) and triclinic  $P1$  (16 examples). This distribution of space group is not very different from that already noted for diverse organic molecules crystallizing in non-centrosymmetric space groups.<sup>16,17</sup> Consideration of the modes of helix association, leading to a critical nucleus, can provide insights into the growth of helical peptide crystals. Almost all observed structures display a head-to-tail arrangement of helices in columns, since both  $3_{10}$  and  $\alpha$  helical peptides possess free donor and acceptor groups capable of hydrogen bonding at both ends of the molecule.<sup>11</sup> Such an arrangement can be in register, as illustrated in Figure 6, or mediated by solvent molecules, most often water or alcohols, as in the case of polymorphs **Ic** and **Id** in Figure 4.

Dimer formation must necessarily precede nucleation. In the case of cylindrical helical structures two modes of association, parallel or antiparallel, may be considered. Lateral association requires favorable interactions between helix faces. For apolar peptide helices, crystallization is often accomplished from alcohol solutions containing varying amounts of water. Formation of hydrogen-bonded head-to-tail dimers is unlikely to be favored because of solvent competition for donor and acceptor sites. Lateral helix association may be driven in an entropic

**TABLE 2: Backbone and Side Chain Torsion Angles (deg) for Peptide I in Four Polymorphic Crystals<sup>a</sup>**

residue	<b>Ia</b>			<b>Ib</b>			<b>Ic</b>			<b>Id</b> (Mol. 1)			<b>Id</b> (Mol. 2)		
	$\phi$	$\psi$	$\omega$	$\phi$	$\psi$	$\omega$	$\phi$	$\psi$	$\omega$	$\phi$	$\psi$	$\omega$	$\phi$	$\psi$	$\omega$
Leu(1)	−65.1	−40.0	−177.6	−65.0	−53.5	−159.4	−71.0	−39.0	178.8	−62.3	−40.5	−174.3	−70.6	−38.9	−175.0
Aib(2)	−56.4	−45.1	−179.3	−58.4	−40.7	−173.9	−57.0	−45.0	−176.5	−58.9	−42.0	179.1	−58.0	−44.5	178.7
Phe(3)	−71.0	−40.6	178.9	−73.0	−23.5	172.8	−69.0	−38.0	177.0	−71.1	−39.6	−178.9	−68.1	−41.1	−178.5
Phe(4)	−54.3	−46.0	179.4	−72.3	−30.8	171.9	−59.0	−42.0	176.7	−58.8	−44.0	175.5	−58.7	−40.9	176.8
Leu(5)	−69.6	−48.6	179.7	−65.8	−50.9	179.3	−73.0	−40.0	171.3	−68.0	−45.1	179.2	−74.6	−42.5	179.7
Aib(6)	−54.0	−43.8	−174.5	−52.9	−50.2	−174.0	−56.0	−28.0	−175.8	−53.2	−38.3	−175.0	−54.6	−36.4	−176.1
Ala(7)	−60.2	−34.6	−177.9	−64.0	−39.0	−178.7	−63.0	−16.0	178.2	−61.2	−19.3	175.6	−62.1	−16.1	175.0
Ala(8)	−66.3	−30.8	178.4	−68.3	−35.2	176.0	−68.0	−13.0	−179.2	−66.0	−14.0	171.3	−61.5	−26.6	−178.1
Leu(9)	−89.0	−45.1	−176.1	−72.5	−37.9	177.8	−100.0	7.0	169.0	−67.2	−25.0	−177.4	−65.8	−42.1	−178.2
Aib(10)	52.0	44.0	178.7	56.5	39.2	176.0	59.0	35.0	176.0	47.1	44.3	−176.0	50.0	38.8	−177.0
side chain	$\chi^1$		$\chi^2$		$\chi^1$		$\chi^2$		$\chi^1$		$\chi^2$		$\chi^1$		$\chi^2$
Leu(1)	−168.0		−179.9, 54.5		−74.9		167.9, −71.7		−178.0		−178.5, 56.0		−173.7		−174.6, 64.8
Phe(3)	−73.8		80.0, −101.5		−79.3		78.6, −99.5		−67.2		74, −105.7		−75.6		73.2, −110.5
Phe(4)	−171.3		92.8, −87.9		−79.8		85.9, −92.4		−167.3		85.5, −97.0		−169.2		69.2, −111.4
Leu(5)	−66.4		170.2, −67.0		173.8		179.2, 55.3		−70.0		173.3, −63.0		−66.7		172.6, −68.2
Leu(9)	−176.8		−171.6, 65.5		−63.2		175.9, −57.0		−62.0		−169, −49		−73.7		166.2, −69.0

<sup>a</sup> Estimated standard deviations  $\approx 0.7^\circ$  (**Ia**),  $0.5^\circ$  (**Ib**),  $2^\circ$  (**Ic**), and  $1^\circ$  (**Id**).



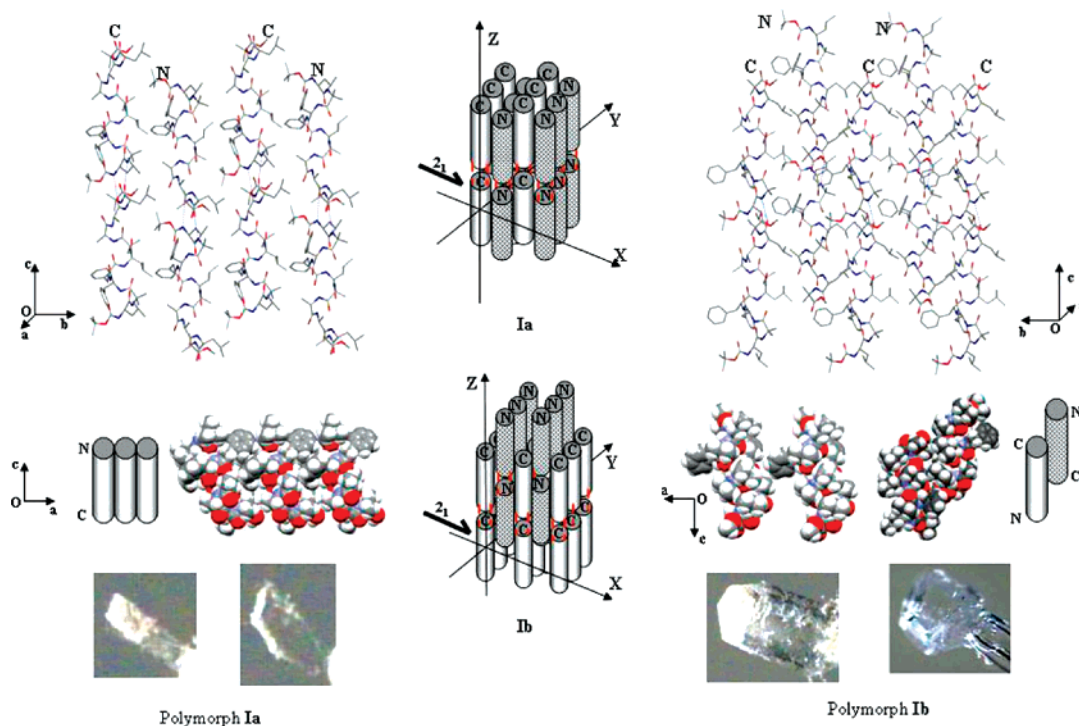


**Figure 3.** Two examples of monoclinic crystal forms ( $P2_1$ ) in the decapeptide Boc-Leu-Aib-Phe-Phe-Leu-Aib-Ala-Ala-Leu-Aib-OMe **I**. In both polymorphs the crystallographic  $2_1$  screw lies perpendicular to the helix axis, along the  $X$  direction. Inspection of the placement of molecules in the crystallographic unit cell indicates that the helix axis lie parallel to the  $c$  axis. The association of raftlike structures formed by close packing of translationally related molecules into a critical nucleus for crystal formation is schematically illustrated using a smooth cylinder as an approximation for the rodlike peptide helices. Space-filling views of translationally related molecules are shown. Two views of the crystals obtained at approximately right angles to one another are shown.

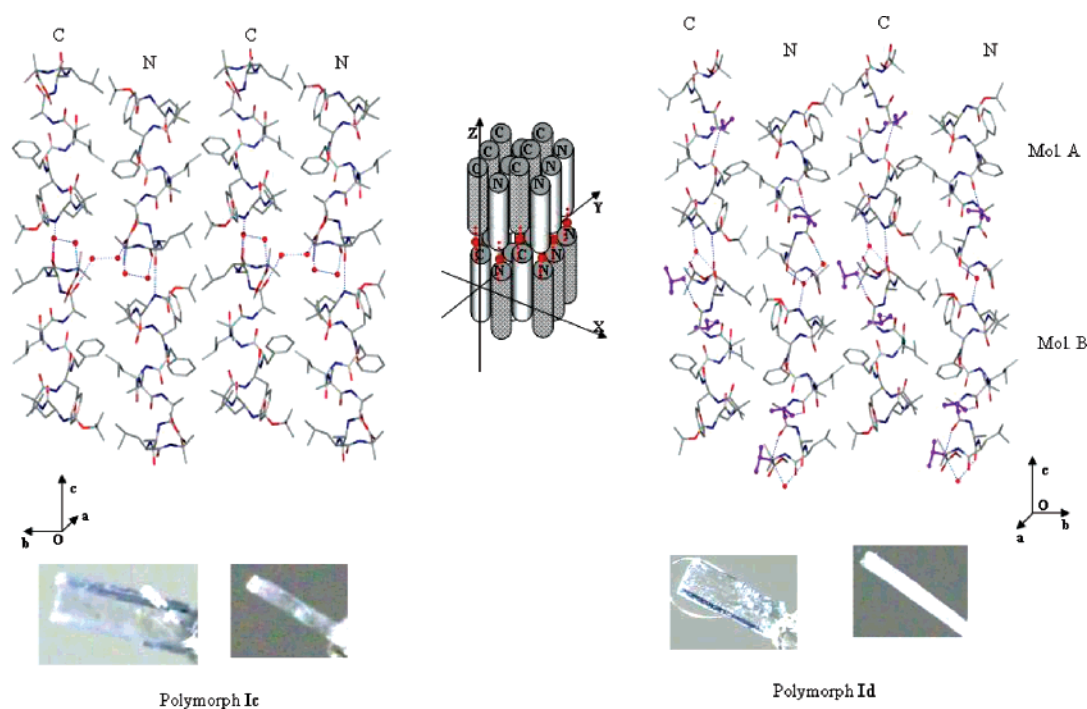


**Figure 4.** Examples of solvated orthorhombic (**Ic**) and monoclinic (**Id**) crystal forms of the decapeptide Boc-Leu-Aib-Phe-Phe-Leu-Aib-Ala-Ala-Leu-Aib-OMe, **I**. In the monoclinic polymorph the crystallographic  $2_1$  screw lies perpendicular to the helix axis, along the  $X$  direction. Inspection of the placement of molecules in the crystallographic unit cell indicates that the helix axis lie parallel to the  $c$  axis. The association of translationally related molecules into rafts and build-up of the crystal structure is schematically illustrated. Two orthogonal views of the crystals are illustrated. The nonstandard setting of the orthorhombic form  $P22_12_1$  has been chosen instead of  $P2_12_12$  to facilitate comparisons with the three monoclinic polymorphs.

sense by solvophobic effects, which arise due to the liberation of interacting solvent molecules, a feature observed for organic structures with large surface area.<sup>18</sup> Dispersion interactions

between apolar side chains can also contribute favorably, enabling association into raftlike structures, in which the shortest dimension corresponds to the length of the molecule ( $\sim 15$  Å

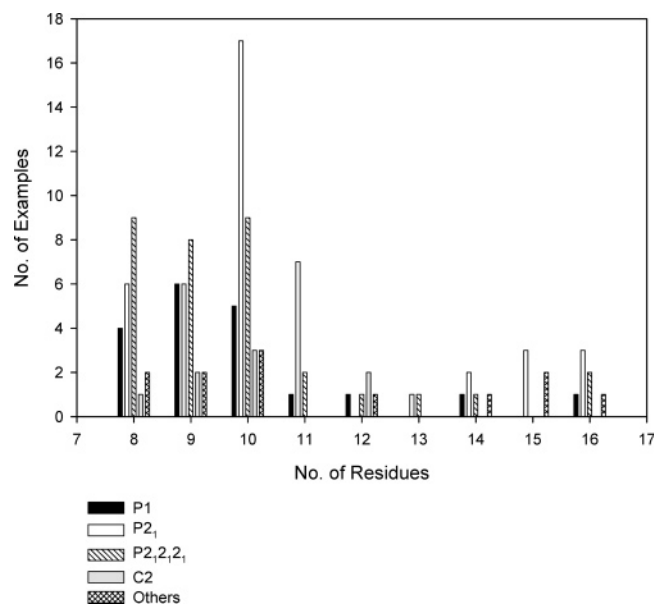


**Figure 5.** The distribution of space groups observed in crystal structures of apolar helical peptides with sequence length  $\geq 8$  residues, from the Cambridge Structural Database (Total observations = 117). The number of observations are (residue/examples):  $P1$ , 8/4, 9/6, 10/5, 11/12, 14/16, 1/13, 15/0;  $P2_1$ , 8/6, 9/6, 10/17, 11/7, 12/0, 13/1, 14/2, 15/16, 3;  $P2_12_12_1$ , 8/9, 9/8, 10/9, 11/2, 12/13, 14/1, 15/0, 16/2;  $C2$ , 8/1, 9/2, 10/3, 11/0, 12/2, 13/14, 15/16, 0. Others:  $P2$ , 12/1;  $C222_1$ , 8, 10, 15/1;  $P2_12_12_1$ , 8/1, 9/2, 10, 16/1;  $P4_3$ , 14/1;  $P4_1$ , 15/1;  $P4_32_12$ , 10/1. In a few cases of achiral peptide structures, the  $P1$  and  $P2_1/c$  space groups have been combined with  $P1$  and  $P2_1$ , respectively.

in the case of a 10-residue  $\alpha$ -helix (Figure 7). The combination of rafts is favored by the burying of a large surface area, once again, due to solvophobic forces. Embryonic nuclei can then be generated by growth in directions perpendicular to the helix axis, resulting in blocklike structures. Association of blocks in the third dimension via hydrogen bond formation permits growth of the nucleus in the third dimension.

Crystals in the triclinic space group  $P1$  are readily generated by stacking rafts in parallel fashion (Figure 7b). Each molecule is translationally related to its neighbors. Two distinct  $P1$  forms can arise by different modes of assembly of rafts. In-register stacking will give rise to the parallel square grid packing arrangement, which has been observed in several triclinic crystals of peptide helices. In this case each molecule makes close contacts with four neighbors. Slippage of two adjacent layers of rafts creates the parallel pseudo-hexagonal arrangement in which each molecule is surrounded by six equivalent neighbors.<sup>11</sup> An antiparallel dimer containing a 2-fold rotation axis may be used to generate the space group  $P2$  (Figure 7c). Curiously, only one example for a peptide helix crystallizing in  $P2$  is observed in the database (CSD code: ADUJEO). Interestingly, this structure contains some unusually small contact distances between non-hydrogen atoms. A simulation of protein crystal nucleation also reveals a considerable discrepancy between the frequency of occurrence of  $P2$  in simulations and in the database.<sup>19</sup> If distortions occur from perfect antiparallel orientations of the two helices, the resultant translationally generated structure is in space group  $P1$  with two molecules in the asymmetric unit. Notably, in the peptide helix data set used in the present study, there are 7 examples of structures in  $P1$  with multiple molecules in the asymmetric unit. The relative infrequency of the occurrence of  $P2$  may be ascribed to inefficient side-chain packing, in the case of in-register arrays in which all adjacent helices are antiparallel. This may be contrasted with the case of two-dimensional crystals,

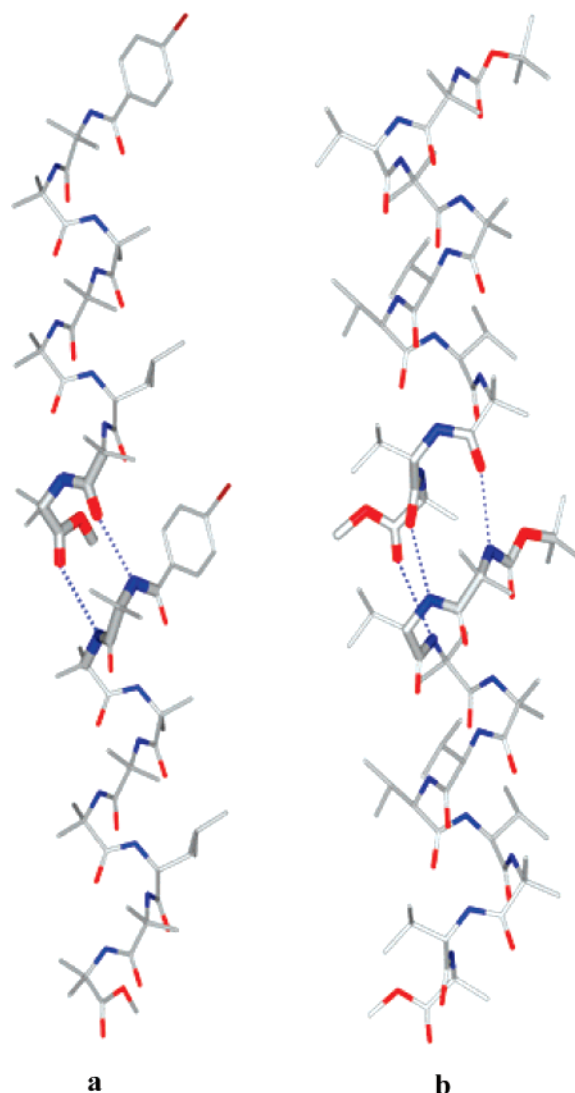


**Figure 6.** Examples of ideal in-register head-to-tail hydrogen bonding resulting in long cylindrical helical columns. The backbone in the head-to-tail region has been enlarged in size. (a)  $3_{10}$  helix association (2 exposed N-H groups) in crystals of pBrBz-(Aib)<sub>5</sub>-Leu-(Aib)<sub>2</sub>-OMe.<sup>28</sup> (b)  $\alpha$ -Helix association (3 exposed N-H groups) in crystals of Boc-Aib-Val-Aib-Aib-Val-Val-Val-Aib-Val-Aib-OMe (molecule A).<sup>29</sup> Imperfect registry results in solvation of the interhelix head-to-tail region in crystals. Note in all cases, the number of C=O groups exceeds the number of N-H groups by 1 because of the contribution from the N-terminal blocking group.

where the plane group  $P2$  has the highest occurrence.<sup>20</sup> Stacking of rafts generated from an antiparallel dimer with a 2-fold symmetry axis facilitate packing, generating a  $2_1$  screw axis in a direction perpendicular to the helix axis. Formation of monoclinic crystals can then be readily visualized by displaced stacking of rafts in both parallel and antiparallel fashion (Figure 7d). The resultant embryonic nuclei will now contain “upper and lower surfaces” in which hollows and projections alternate. Lego set fitting of blocks by head-to-tail hydrogen-bonding results in growth of the nucleus along the direction of helix axis. These modes of association readily generate structures with  $2_1$  axis, which can be oriented either parallel or perpendicular to the helix axis.

All three monoclinic polymorphs of peptide **I** correspond to a perpendicular orientation of the helices with respect to the  $2_1$  screw axis. Polymorphs **1a** and **1b** could be formally described by different extents of slippage of two adjacent rafts along the direction of the helix axis. If two symmetry related molecules

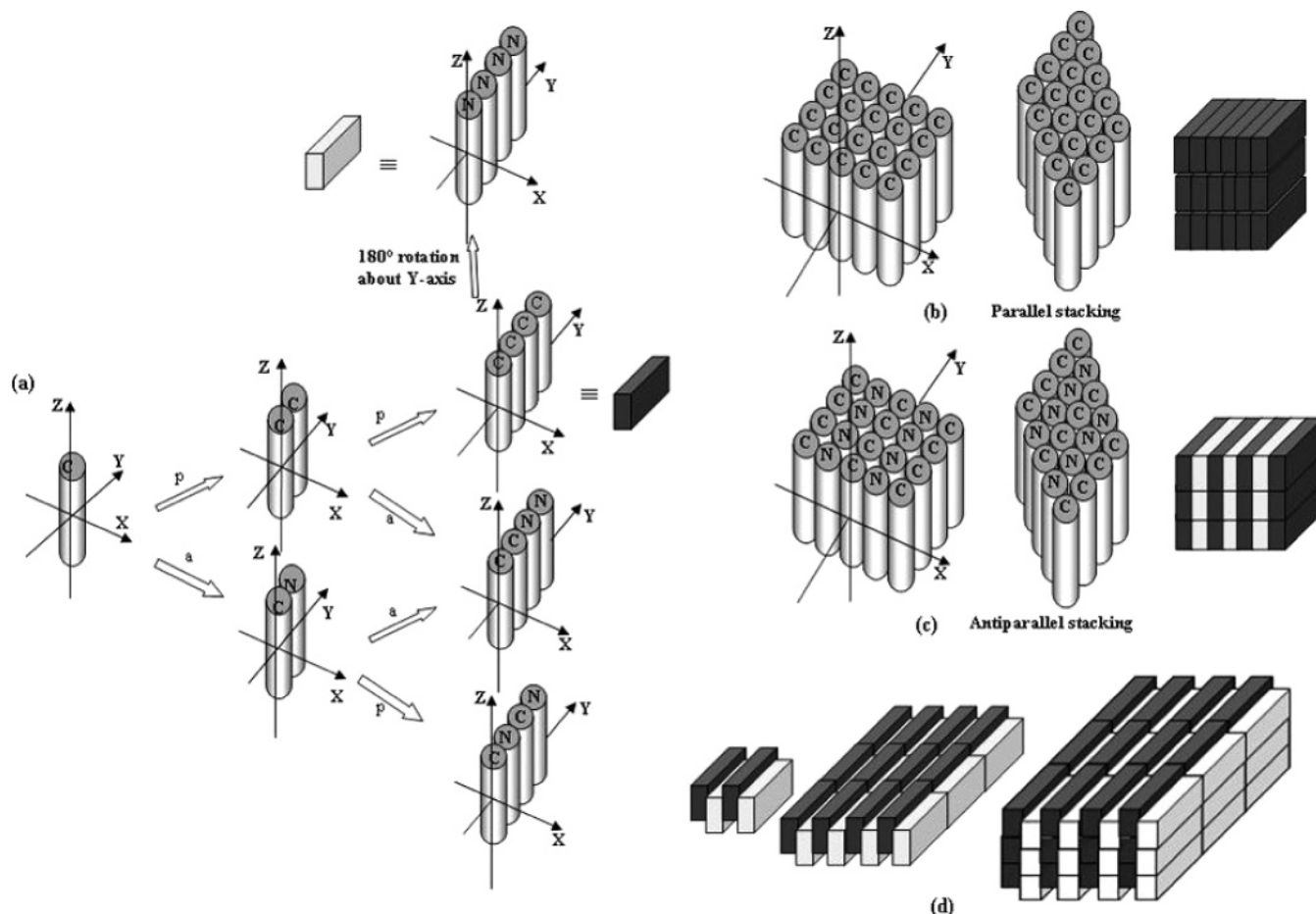


**Figure 7.** Crystal nucleation model. (a) Schematic view of self-association of rodlike helical molecules to form raftlike structures and subsequent growth of the critical nucleus in three dimensions. For convenience, cylinders are oriented with the helix axis running parallel to the Z axis. Both parallel (p) and antiparallel (a) dimer formations are considered. (b) Parallel stacking of rafts leading to space group  $P1$  in (left) square grid and (right) pseudohexagonal arrangements. In the square-grid arrangement, helices are registered in both X and Y directions, with each molecule contacting four nearby helices. In the pseudohexagonal arrangement, slippage of adjacent rafts occurs in a direction perpendicular to the helix axis, resulting in a close packed structure, in which each molecule is surrounded by six helices. In peptide helices, interactions between projecting side chains may be expected to determine the precise nature of packing. (c) The antiparallel arrangement can grow along the Z direction, by interactions with the translationally related blocks to yield the infrequently observed space group  $P2$ . (d) Displaced stacking of rafts for the formation of monoclinic and orthorhombic crystals: (left) antiparallel displaced stacking of rafts in the X direction, (middle) growth in the second direction (Y axis) to form a blocklike structure, and (right) Lego set fitting of blocks in the third direction (Z axis) with the formation of head-to-tail hydrogen bonds.

are considered, this would correspond to a displacement of the position of the  $2_1$  screw axis in the direction of the long axis of the helix. Both polymorphs **1a** and **1b** do not contain any solvent molecules, with head-to-tail registry being maintained by intermolecular hydrogen bonds. In **1a**, the translationally related raft is readily generated by close packing of molecules in the Y direction (crystallographic *a* axis). In contrast, in **1b** translationally related molecules along the Y direction are not close-packed because of the projecting Phe side chain (Figure 3). Raft formation must therefore be preferred using adjacent antiparallel slipped molecules along the X direction (crystallographic *b* axis). This would generate a raft with irregular edges containing both projections and hollows, a relatively rare situation in all the helical peptides analyzed. Such an embryo should grow rapidly in a process driven by the imperative of minimizing exposed surface area in a manner that propagation of the nucleus occurs with more or less equal rates along the three directions. Inspection of the crystal dimensions in the case of **1a** (Table 1,  $0.22 \times 0.15 \times 0.02 \text{ mm}^3$ ) and **1b** (Table 1,  $0.33 \times 0.26 \times 0.13 \text{ mm}$ ) suggest preferential growth in two dimensions, which would correspond to the X and Y directions in the schematic model of association. Interestingly, there is a significant difference in the ratio of the shortest to the longest crystal

dimension in the case of **1a** and **1b**. Although polymorphs **1c** and **1d** belong to crystallographically distinct space groups ( $P2_12_1$  and  $P2_1$ ), both the helix aggregates are identical suggesting crystal growth proceeds from a common nucleus structure. The sole difference is in piling two-dimensional blocks along the Z-axis (helix axis) direction by head-to-tail hydrogen bonding. The solvent molecules trapped in the head-to-tail region in the two cases are different; two water molecules in **1c** and one water and one isopropanol molecules in **1d**. **1d** then reduces to a situation in which the crystallographic asymmetric unit contains two independent molecules that are indeed related by a pseudo  $2_1$  screw axis. In both cases, inspection of the crystal dimensions suggest widely differing rates of propagation of the nucleus, with one dimension being significantly smaller.

The initial step in the crystallization process is molecular association driven by solvent forces. Desolvation is favored when large complementary molecular surfaces are brought into contact. The solvophobic effect<sup>21,22</sup> is undoubtedly a combination of both solvent entropy factors and the favorable enthalpies gained as a result of multiple dispersive (van der Waals) interactions. Surface complementarity undoubtedly determines the nature of association.<sup>17</sup> In the large number of helical peptides that have been crystallized, a variety of nonpolar side



chains of differing shape and volume are observed. Approximating these molecules as smooth cylinders is convenient in analyzing potential models for conversion of a solution phase aggregate into a single crystal, constrained by space group symmetries. Molecular rafts provide an embryonic structure, which can then be built in modular fashion into a nucleus, which possesses all the symmetry elements of the crystal, its dimension lying in 10–100-nm range. For peptide helices of the type considered here, nonpolar interactions are present exclusively in two dimensions, while hydrogen bonding occurs in the third dimension, in a direction parallel to the axis of the helix. The assembly of boxes, with a thickness approximately one helix length (15–20 Å), that grow in two dimensions promoted by solvophobic interactions, into the third dimension by stacking using multiple hydrogen-bonding interactions appears to be an attractive model for crystal growth. Phenomena like crystal twinning, the occurrence of morphologically attractive crystals, which do not provide sharp X-ray diffraction patterns and the frequent occurrence of polymorphic forms, may be readily rationalized. The development of a “grammar for crystal packing”<sup>17</sup> may require careful analysis of the structures of molecules which have large apolar surface areas and limited hydrogen-bonding potential directed along specific molecular axes. Although we have used a “smooth cylinder” representation as an approximation of the rodlike molecules considered in this study, the specific close-packed aggregates may be formed from a variety of irregularly shaped molecules. The identification of embryonic molecular aggregates, which initiate the formation of critical nuclei, is aided by careful inspection of near neighbor interactions in high-resolution crystal structures. Viewing the crystal as a molecular aggregate unconstrained by projections down specific unit cell axes is helpful, a strategy that has been advanced for the comparison of polymorphic structures.<sup>23</sup> Detailed atomic and molecular models for crystallization nuclei may also be valuable in generating initial models for nanoscale structures in which the repetitive lattice is restricted to a limited space of the bulk material.<sup>24</sup> A structural understanding of nascent nuclei may also facilitate attempts to impede crystallization, promoting “the dark side of crystal engineering” in the design of glasses and liquid crystalline materials.<sup>25</sup>

## Conclusions

Nucleation and growth of crystals is undoubtedly a phenomenon that is governed by a complex interplay of kinetic and thermodynamic factors. By analogy with views on protein folding, speed of formation and stability of structure often go hand in hand.<sup>26</sup> Long-lived nascent nuclei, which must be characterized by favorable free-energy processes will necessarily have a higher probability of growth by addition of a raftlike or blocklike structure. Beyond the critical size, the nucleus is committed to crystal formation. The occurrence of multiple polymorphic forms and the frequent observation of concomitant

polymorphs,<sup>27</sup> in the case of molecules with large surface areas like proteins, suggest that the energy landscape for molecular association is best represented by a broad and ruggedly shaped minimum, allowing the population of aggregate nuclei with distinctly different packing arrangements.

**Acknowledgment.** We thank Dr. A. Sriranjini for the sample of the peptide. P.G.V. thanks the Council of Scientific and Industrial Research, India, for award of a Senior Research Fellowship. This research was supported by a program grant from the Department of Biotechnology, Government of India, and a grant from the Council of Scientific and Industrial Research, India. X-ray diffraction data were collected on the CCD facility funded under the IRHPA program of the Department of Science and Technology, India.

## References and Notes

- (1) Mullin, J. W. *Crystallization*, 4th ed.; Butterworth-Heinemann: Oxford, 2001.
- (2) Oxtoby, D. W. *Acc. Chem. Res.* **1998**, *31*, 91.
- (3) Yau, S.-T.; Vekilov, P. G. *Nature* **2000**, *406*, 494.
- (4) Dunitz, J. D.; Bernstein, J. *Acc. Chem. Res.* **1995**, *28*, 193.
- (5) Aravinda, S.; Shamala, N.; Roy, R. S.; Balaram, P. *Proc. Indian Acad. Sci. (Chem. Sci.)* **2003**, *115*, 373.
- (6) Venkatraman, J.; Shankaramma, S. C.; Balaram, P. *Chem. Rev.* **2001**, *101*, 3131.
- (7) Prasad, B. V. V.; Balaram, P. *CRC Crit. Rev. Biochem.* **1984**, *16*, 307.
- (8) Karle, I. L.; Balaram, P. *Biochemistry* **1990**, *29*, 6747.
- (9) Toniolo, C.; Benedetti, E. *Trends Biochem. Sci.* **1991**, *16*, 350.
- (10) Toniolo, C.; Benedetti, E. *Macromolecules* **1991**, *24*, 4004.
- (11) Karle, I. L. *Acta Crystallogr.* **1992**, *B48*, 341.
- (12) Thompson, D. *On Growth and Form*; Bonner, J. T., Ed.; Cambridge University Press: 1961; Canto edition, 1997, p 170.
- (13) Schneider, T. R.; Sheldrick, G. M. *Acta Crystallogr.* **2002**, *D58*, 1772.
- (14) Sheldrick, G. M. *SHELXL-97, A program for crystal structure refinement*; University of Göttingen: Göttingen, 1997.
- (15) Spek, A. L. *J. Appl. Crystallogr.* **2003**, *36*, 7.
- (16) Mighell, A. D.; Himes, V. L. *Acta Crystallogr.* **1983**, *A39*, 737.
- (17) Brock, C. P.; Dunitz, J. D. *Chem. Mater.* **1994**, *6*, 1118.
- (18) Zhao, Y.; Moore, J. S. *Foldamers: Structure, Properties and Applications*; Hecht, S., Huc, I., Eds; Wiley-VCH Verlag GmbH & Co.: New York, 2007; p 75.
- (19) Pellegrini, M.; Wukovitz, S. W.; Yeates, T. O. *Prot. Struct. Funct. Genet.* **1997**, *28*, 515.
- (20) Plass, K. E.; Grzesiak, A. L.; Matzger, A. J. *Acc. Chem. Res.* **2007**, *40*, 287.
- (21) Ray, A. *Nature* **1971**, *231*, 313.
- (22) Yaacobi, M.; Ben-Naim, J. *J. Phys. Chem.* **1974**, *78*, 175.
- (23) Bernstein, J. *Polymorphism in Molecular Crystals*; Oxford University Press: 2002.
- (24) Billinge, S. J. L.; Levin, I. *Science* **2007**, *316*, 561.
- (25) Lebel, O.; Maris, T.; Perron, M.-E.; Demers, E.; Wuest, J. D. *J. Am. Chem. Soc.* **2006**, *128*, 10372.
- (26) Baldwin, R. L. *Nature* **1994**, *369*, 183.
- (27) Bernstein, J.; Davey, R. J.; Henck, J.-O. *Angew. Chem., Int. Ed.* **1999**, *38*, 3440.
- (28) Bavoso, A.; Benedetti, E.; Di Blasio, B.; Pavone, V.; Pedone, C. *J. Biomol. Str. Dyn.* **1988**, *5*, 803.
- (29) Karle, I. L.; Flippen-Anderson, J. L.; Uma, K.; Balaram, H.; Balaram, P. *Proc. Natl. Acad. Sci. U.S.A.* **1989**, *86*, 765.